

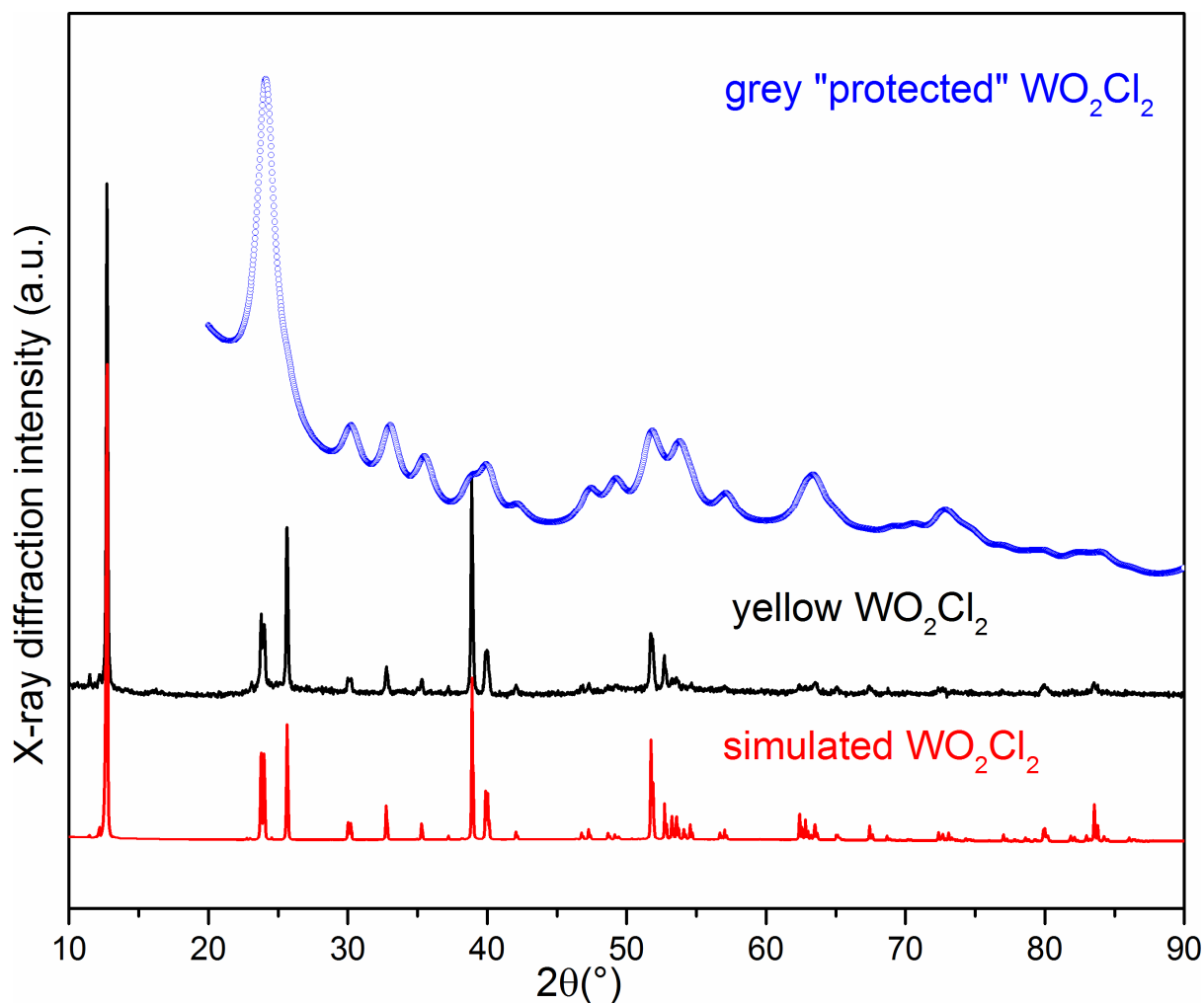
Synthesis of a Highly Reactive Form of WO_2Cl_2 , its Conversion into Nanocrystalline Mono-Hydrated WO_3 and Coordination Compounds with Tetramethylurea

Marco Bortoluzzi, Claudio Evangelisti, Fabio Marchetti, Guido Pampaloni, Fabio Piccinelli, Stefano Zacchini

Supporting Information

<u>Table of contents</u>	<i>Page</i>
Figure S1. P-XRD patterns of orthorhombic WO_2Cl_2 , yellow WO_2Cl_2 and grey WO_2Cl_2	S2
Figure S2. Representative HR-TEM micrograph of yellow WO_2Cl_2	S3
Figure S3. Comparative view of P-XRD patterns	S4
Figure S4. Representative micrograph and selected area electron diffraction (SAED) pattern of light green $\text{WO}_3 \cdot \text{H}_2\text{O}$ (from grey WO_2Cl_2)	S5
Figure S5. Representative HR-TEM micrograph of lemon yellow $\text{WO}_3 \cdot \text{H}_2\text{O}$ (from yellow WO_2Cl_2)	S6
Table S1. Computed average Mayer bond orders (C-PCM/ ω B97X) for the W–O interactions in 1	S7
Figure S6. DFT C-PCM/ ω B97X calculated structure of 2	S8

Figure S1. P-XRD patterns of: orthorhombic WO_2Cl_2 (space group $Immm$; simulated from PDF 01-081-2322, red line); commercial yellow WO_2Cl_2 (black line); grey WO_2Cl_2 protected from the moisture with a thin layer of inert paraffin oil (blue line).



The *blue line* pattern has been cut in the 10-20° 2θ range, due to the presence of a very broad peak ascribable to the paraffin oil. The paraffin oil is responsible also for the broadened profile of the diffraction peaks.

Figure S2. Representative HRTEM micrograph of commercial (yellow) WO_2Cl_2 .

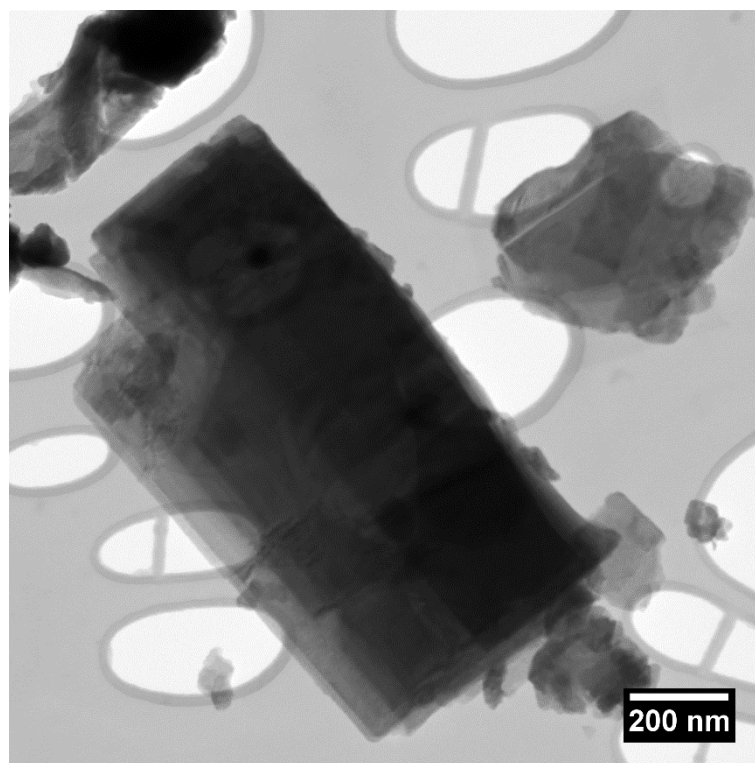


Figure S3. Comparative view of the P-XRD patterns of the solid materials obtained from: grey WO_2Cl_2 , after air exposure for 3 days (red line); grey WO_2Cl_2 , after air exposure for 10 minutes (black line); yellow WO_2Cl_2 , after air exposure for 3 days (blue line).

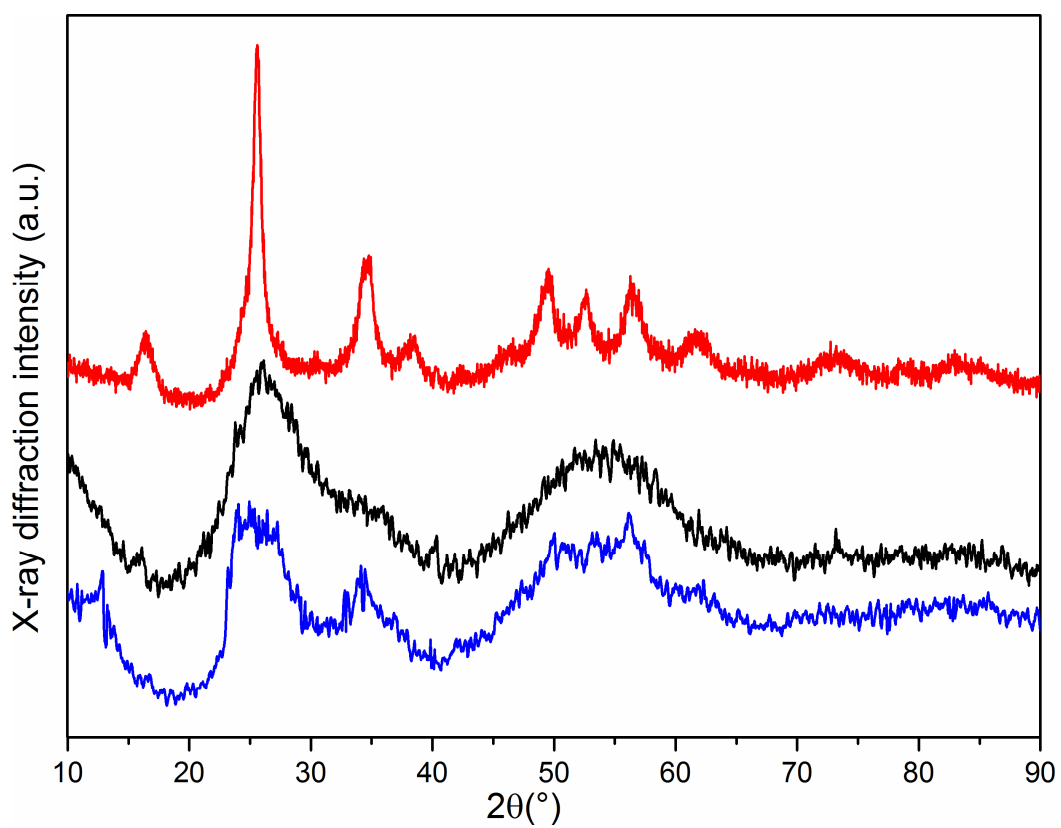


Figure S4. Representative micrograph (left side) and selected area electron diffraction (SAED) pattern (right side) of $\text{WO}_3 \cdot \text{H}_2\text{O}$ (light green solid, from hydrolysis of grey WO_2Cl_2).

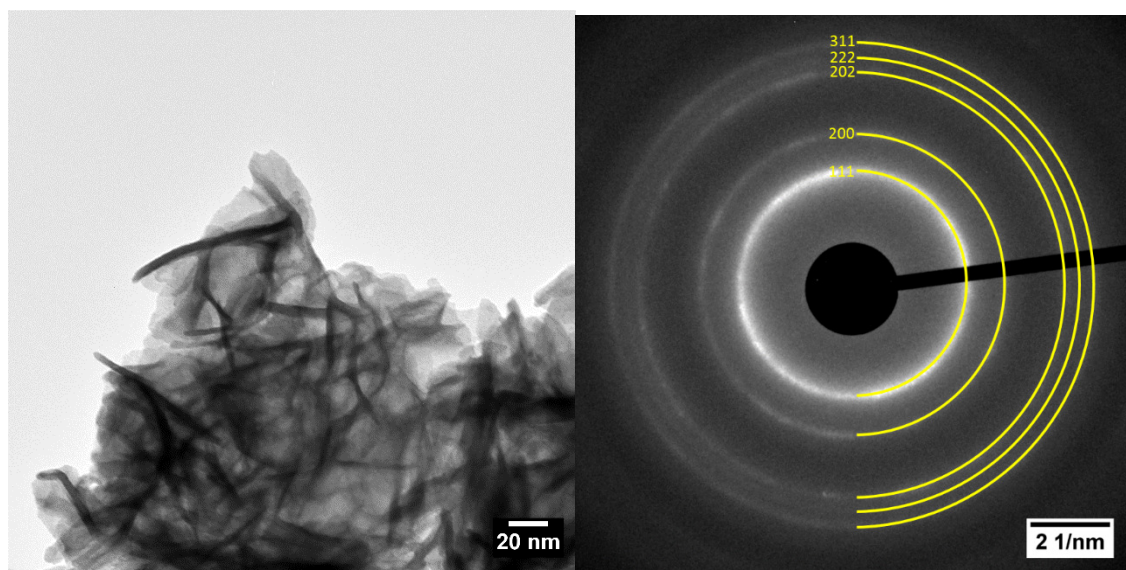


Figure S5. Representative HRTEM micrograph of $\text{WO}_3 \cdot \text{H}_2\text{O}$ (lemon yellow solid, from hydrolysis of commercial yellow WO_2Cl_2).

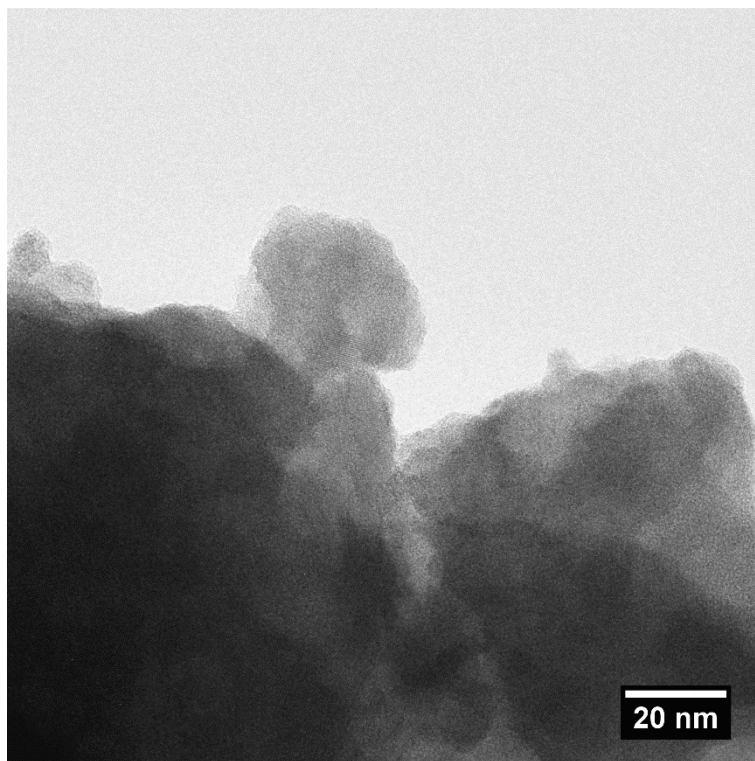


Table S1. Computed average Mayer bond orders (C-PCM/ ω B97X) for the W–O interactions in **1**.

W=O(terminal)	1.933
W=O(bridging)	1.444
W–O(bridging)	0.310
W–O(tmu)	0.507

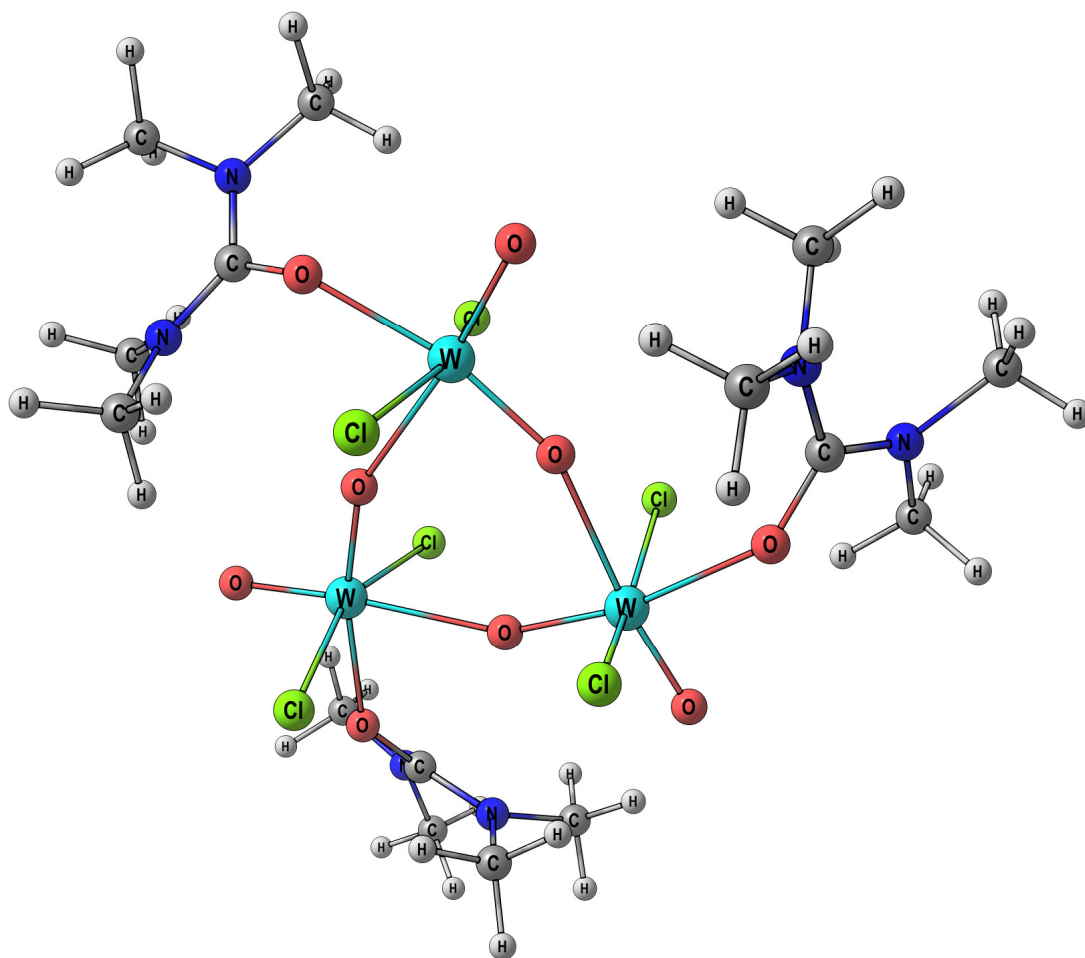


Figure S6. DFT C-PCM/ ω B97X calculated structure of $\text{WO}_2\text{Cl}_2(\text{tmu})_2$, **2**. Dichloromethane as implicit solvent.

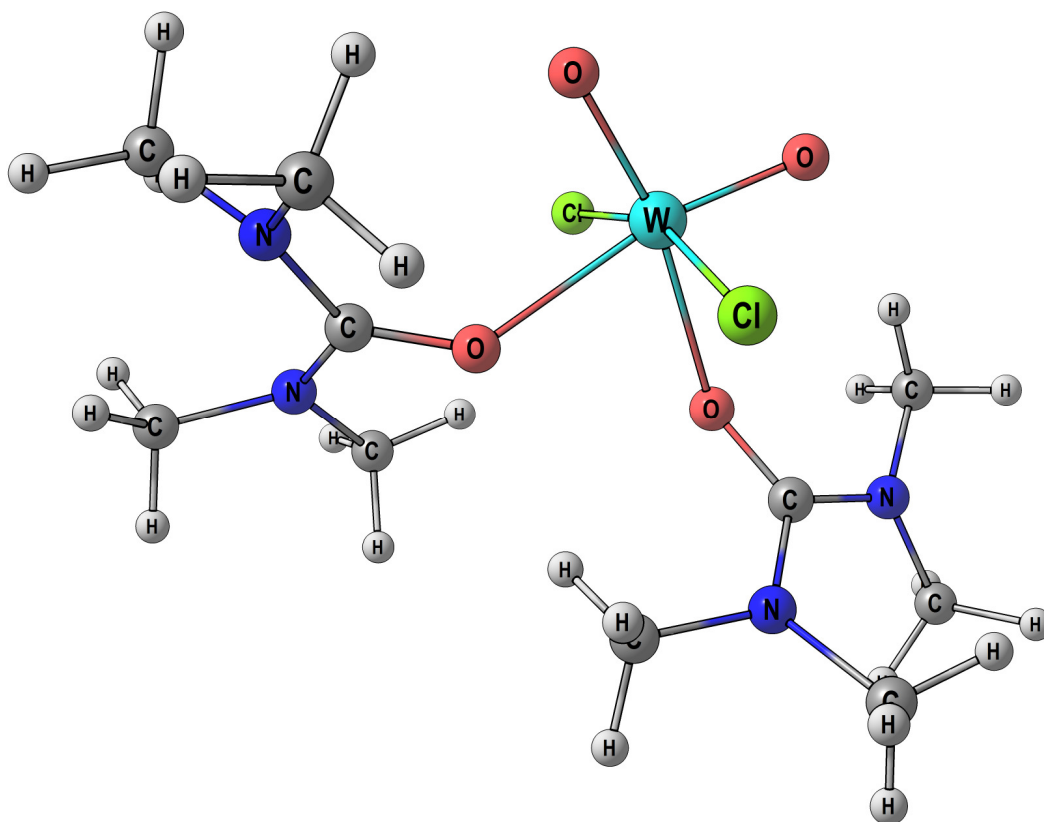


Table S2. Selected computed bond lengths (Å) and angles (°) for $\text{WO}_2\text{Cl}_2(\text{tmu})_2$, **2**.

Bond		Angle	
W=O	1.686	O=W=O	102.2
	1.690	O=W-O	90.3
W-O	2.213		90.9
	2.185		166.8
W-Cl	2.398		167.4
	2.399	O=W-Cl	95.2
C=O	1.271		96.2
	1.272		95.7
			95.2
		C=O-W	134.7
			140.6